J. Fluid Mech. (2009), *vol.* 639, *pp.* 195–211. © Cambridge University Press 2009
doi:10.1017/S0022112009990954

Destructive interactions between two counter-rotating quasi-geostrophic vortices

JEAN N. REINAUD† AND DAVID G. DRITSCHEL

Mathematical Institute, University of St Andrews, North Haugh, St Andrews KY16 9SS, UK

(Received 23 April 2008; revised 26 June 2009; accepted 26 June 2009; first published online 5 October 2009)

This paper illustrates the linear stability and the nonlinear evolution of two opposite-signed quasi-geostrophic vortices. We investigate the influence of the volume ratio between the two vortices as well as the influence of their vertical offset. Instability is always found for sufficiently close vortices. A convenient measure of the separation distance between the two vortices at their margin of stability is the horizontal gap between their two outermost edges. When the vortex volume ratio is very close to unity, the critical gap at the margin of stability tends to increase with the vertical offset. However, for volume ratios greater than 1.1, it decreases with the vertical offset. This is due to differences in the magnitude of the tilt angle of the vortices. The nonlinear evolution of unstable equilibria tends to be destructive, often breaking one vortex or both vortices into smaller vortices.

1. Introduction

Vortices or coherent and compact volumes of anomalous potential vorticity (PV) – together with jets – dominate the fluid motion in the Earth's oceans and atmosphere at medium-to-synoptic scales (see Holton *et al.* 1995; Garrett 2000). Vortices are ubiquitous features, and for example Ebbesmayer *et al.* (1986) estimated that between 1000 and 10 000 vortices populate the upper layers of the North Atlantic alone. Understanding how these vortices interact is therefore essential for understanding complex atmospheric and oceanic flows. Such flows are strongly influenced by the Earth's rotation and by the largely stable stratification of the fluid. These two dominant effects lead to a nearly layer-wise two-dimensional motion, parallel to isopycnal surfaces. In this paper we use the simplest dynamical model which takes into account these effects, the quasi-geostrophic (QG) model (see e.g. Vallis 2006 for further details).

It is known that QG turbulence exhibits an 'inverse' energy cascade in spectral space; that is, statistically, energy flows from high wavenumbers to smaller ones (see e.g. Hua & Haidvogel 1986). It has been argued that this cascade may be related, in physical space, to the merger of co-rotating vortices. Vortex merger under the QG approximation has been extensively addressed in the literature (see e.g. von Hardenberg *et al.* 2000; Dritschel 2002; Reinaud & Dritschel 2002, 2005; Bambrey, Reinaud & Dritschel 2007; Ozugurlu, Reinaud & Dritschel 2008). These studies showed that two co-rotating vortices may strongly interact and sometimes lead to the formation of moderately larger vortices. Yet these interactions also generate many secondary smaller vortices as well as vorticity debris and filaments. As shown by

† Email address for correspondence: jean@mcs.st-and.ac.uk

https://doi.org/10.1017/S0022112009990954 Published online by Cambridge University Press

Bambrey *et al.* (2007), interactions between equal-PV vortices may contribute, on average, to the inverse energy cascade. The situation is less obvious when considering co-rotating vortices of unequal PV, as the largest vortex may decrease in size after a strong interaction if its strength (volume integral of the PV) is less than that of the smaller vortex (see Ozugurlu *et al.* 2008).

Turbulent flows additionally involve the interaction between counter-rotating (opposite-signed) vortices. Although interactions between counter-rotating two-dimensional vortices are well understood (see Dritschel 1995 and the references therein), interactions between analogous three-dimensional QG vortices have seldom been considered. Most previous studies have used asymptotic models, where e.g. vortices are approximated by ellipsoids. Those studies concluded that interactions between counter-rotating vortices are not destructive.

Miyazaki, Yamamoto & Fujishima (2003) studied equal-volume counter-rotating vortices using an ellipsoidal moment expansion model. This model excludes non-ellipsoidal deformations (which are part of the full nonlinear dynamics). The authors observed various oscillatory states, which have been independently confirmed in an unpublished study by Reinaud, who used a different reduced model, the ellipsoidal vortex model developed by Dritschel, Reinaud & McKiver (2005).

Miyazaki *et al.* (2003) went on to investigate the interaction of spheroidal counter-rotating vortices in the full QG equations using the contour-advective semi-Lagrangian (CASL) numerical method (Dritschel & Ambaum 1997). In their set-up, the vortices are initially not in equilibrium. The authors observed only weak interactions characterized by stable oscillations or weak filamentation. They concluded that the vortex pairs are robust. However, as shown below, vortices in mutual equilibrium can be squeezed much closer together, allowing for much stronger and destructive interactions.

In this paper, we compute families of equilibrium states (from the full QG equations) for various volume ratios and vertical offsets between the vortices. We restrict attention to opposite-signed vortices having a unit height-to-width aspect ratio, for the sake of simplicity. We address their linear stability and find instability for sufficiently close vortices in every family considered. We then examine the nonlinear manifestation of these instabilities using the contour surgery (CS) numerical method (Dritschel 2002). We find that counter-rotating vortices may in fact break into smaller vortices as a result of their interaction, providing a mechanism that contributes to the direct energy cascade, which evidently coexists in turbulence with the inverse energy cascade.

The paper is organized as follows. We briefly review the formulation of the QG model and the numerical tools used to obtain the equilibrium states and to address their linear stability in § 2. A description of the steady states and the stability analysis is provided in § 3. The nonlinear evolution of unstable vortex pairs is illustrated in § 4, and we conclude in § 5 and present evidence for counter-rotating vortex interactions in QG turbulence.

2. Formulation

2.1. *The QG model*

The QG model used in this study can be obtained from an asymptotic expansion of the Oberbeck–Boussinesq equations for $\epsilon = H/L \ll 1$, where H and L are characteristic vertical and horizontal length scales, and for $Fr \sim Ro \ll 1$, where Fr and Ro are respectively the Froude and Rossby numbers (see e.g. Vallis 2006). Here f is the Coriolis frequency and N is the buoyancy frequency. Following many previous works

https://doi.org/10.1017/S0022112009990954 Published online by Cambridge University Press

(see Reinaud & Dritschel 2005 and the references therein), we take both f and N to be constant for the sake of simplicity.

Stretching the vertical direction by the factor N/f, the governing equations read

$$\frac{\mathrm{D}q}{\mathrm{D}t} = 0, \tag{2.1}$$

$$\Delta\psi = q, \tag{2.2}$$

$$u = -\frac{\partial\psi}{\partial y}, \quad v = \frac{\partial\psi}{\partial x}, \tag{2.3}$$

where q is the QG PV anomaly, ψ is the streamfunction and (u, v) is the horizontal advecting velocity field. In (2.1), $\mathrm{D}/\mathrm{D}t = \partial/\partial t + u\partial/\partial x + v\partial/\partial y$ is the material derivative, and Δ in (2.2) is the three-dimensional Laplace operator. Here, we ignore diabatic heating and viscous diffusion. Hence, as stated in (2.1), the PV is materially conserved. Moreover, the flow is layer-wise two-dimensional (i.e. the motion is tangent to stratification surfaces).

2.2. *Numerical approach*

In this work, we consider vortices of uniform PV, and we use contouradvection-based methods ideally suited to handle sharp PV gradients (or PV jumps) in inviscid QG flows.

We first obtain equilibrium states consisting of two steadily rotating opposite-signed vortices. To this end, we use the numerical method detailed in Reinaud & Dritschel (2002; see in particular their Appendix A). The iterative method forces the PV contours, which enclose the vortices at every height z, to converge to streamlines in the reference frame rotating or translating with the pair of vortices. When this condition is reached, the unperturbed contours do not deform in time and the vortices are in mutual equilibrium.

Next we perform a linear stability analysis of the equilibrium states. The analysis focuses on the deformation modes of the vortex boundaries (see Reinaud & Dritschel 2002 for the details of the formulation). All other modes involving changes to the PV away from the vortex boundaries are neutral. The linear stability analysis corresponds to a complex eigenvalue problem, in which the real part σ_r of the complex eigenvalue σ corresponds to the growth rate of the mode, while their imaginary part σ_i corresponds to the frequency of the mode.

In this study, each contour is discretized by 198 nodes. The largest vortex is spanned by 25 equal-thickness layers in all cases. Both vortices have a unit height-to-width aspect ratio, and the smaller vortex is spanned in the vertical by a number of layers determined by the volume ratio. The total vortex volume V_{tot} in each case is set to $4\pi/3$, implicitly defining the length scale in the problem $\ell = (3V_{tot}/4\pi)^{1/3} = 1$. The time scale is made dimensionless by choosing $q = \pm 2\pi$ inside the vortices. Note that an isolated sphere of the PV q has a rotation period of $6\pi/|q|$.

The equilibrium states are sought in families. A 'family' of equilibria consists of vortex pairs having a prescribed vertical offset and volume ratio between the two vortices. Each equilibrium within the family differs by the horizontal separation between the vortices. We start from vortices relatively distant from one another, and the first guess for the shape of the vortices in the iterative method consists of two spheres. When an equilibrium state is reached, the vortices are slightly pushed together, and the iterative algorithm is resumed for this new separation distance. The stability analysis is performed as described in Reinaud & Dritschel (2002), and we consider 10 azimuthal modes for each contour (sufficient for accuracy).

https://doi.org/10.1017/S0022112009990954 Published online by Cambridge University Press

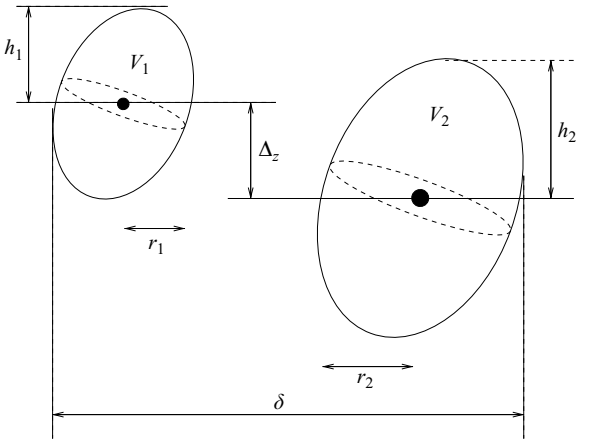


FIGURE 1. General geometry of a vortex equilibrium configuration.

The nonlinear evolution of the vortex pairs is investigated using the CS algorithm developed by Dritschel (2002) for QG flows. This method is purely Lagrangian, and the flow is unbounded. This is consistent with the approach used to obtain the equilibrium states and their stability properties which are also based on explicit contour integration.

3. The equilibrium states

3.1. *General geometry*

We investigate pairs of counter-rotating vortices in mutual equilibrium. Figure 1 illustrates the general geometry of the flow. The vortices have a half-height h_i ($i = 1, 2$) and a mean horizontal radius r_i ($i = 1, 2$). Their volumes are $(4/3)\pi {r_i}^2 h_i$, and without loss of generality we set ${r_1}^2 h_1 + {r_2}^2 h_2 = 1$. As mentioned in the previous section, we limit the study to vortices having a unit height-to-width aspect ratio h_i/r_i. This restriction is justified from simulations of QG turbulence (see e.g. McWilliams, Weiss & Yavneh 1999; Reinaud, Dritschel & Koudella 2003). The volume of the vortices is denoted V_i ($i = 1, 2$), and we denote the volume ratio $\rho_V = V_2/V_1$, taken to be greater than one without loss of generality. In this study, we investigate the following volume ratios: $\rho_V = 1.01, 1.05, 1.1, 1.2, 1.5, 2, 4, 6, 8$ and 10. Note that we disregard the special case $\rho_V = 1$. In this case the global PV centroid is at ∞, and the vortices translate rather than rotate. We ignore this case because finding two opposite-signed vortices of exactly the same volume is highly improbable in e.g. turbulence. Without loss of generality, we assign $q = -2\pi$ to vortex 1 and $q = +2\pi$ to vortex 2. The vertical offset between the two vortices is denoted Δz, and we consider $\Delta z \simeq 0$, 25 % and 50 % of $(h_1 + h_2)$. Without loss of generality, the centre of vortex 1 is placed above that of vortex 2. The horizontal distance between the two vortices is measured by the outermost edge separation distance δ between the two vortices (see figure 1). This parameter monotonically spans the families of equilibria up to and beyond the margin of stability.

3.2. *Equilibrium states and their linear stability*

As mentioned above a family of equilibrium states is characterized by a given volume ratio ρ_V and a vertical offset Δz. We start by computing an equilibrium for distant vortices. When the equilibrium is obtained, we put the vortices closer to one another

https://doi.org/10.1017/S0022112009990954 Published online by Cambridge University Press

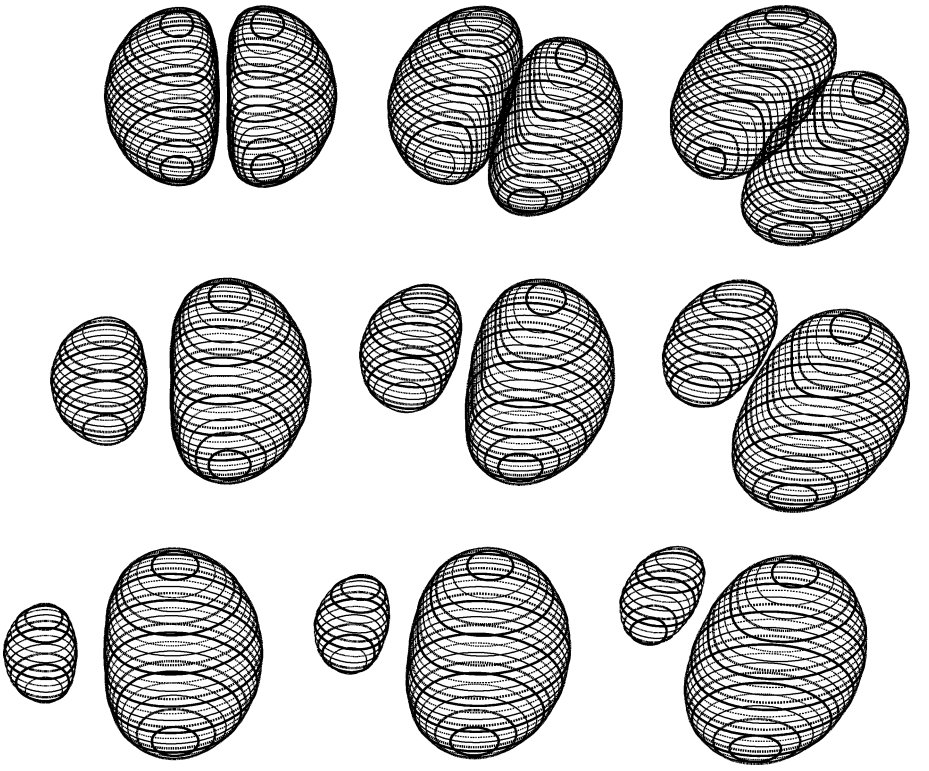


FIGURE 2. Equilibrium states at their margin of stability. From top to bottom, the volume ratios are 1.01, 4 and 10. From left to right the vertical offsets are 0, 25 % and 50 % of $(h_1 + h_2)$.

and resume the procedure. We obtain this way a family of equilibria spanned by their horizontal separation distance. Distant vortices are typically neutrally stable. As the vortices are closer, we eventually reach the margin of stability. The procedure is continued for even closer (unstable) vortices until the algorithm fails to converge towards an equilibrium.

We now examine the shapes of the vortex equilibria and their linear stability. Figure 2 shows the shapes of the vortices at the margin of stability for $\rho_V = 1.01$, 4 and 10 and $\Delta z = 0$, 25 % and 50 % of $(h_1 + h_2)$. The shapes presented here are characteristic of all cases investigated. Notably, the largest vortex (vortex 2) exhibits the greatest deformation (i.e. the largest departure from a spheroidal shape). This is opposite to what happens for co-rotating, equal-PV vortices. This difference stems from the sharply contrasting topology of the flow induced by two co-rotating and two counter-rotating vortices. Similar results are found in two dimensions (see e.g. Dritschel 1995). For horizontally aligned vortices the deformation of the vortices is symmetric with respect to their horizontal midplane. This symmetry breaks as soon as we introduce a vertical offset between the two vortices. In these cases, we observe that the vortices tilt. More than this, the deformation of the vortices is no longer symmetric with respect to their horizontal midsection. In general, symmetry is not representative of these equilibria. These features are more pronounced in figure 3, which shows the last states obtained numerically for the same families, i.e. the equilibria corresponding to the smallest outermost edge separation distance the numerical procedure allowed to

https://doi.org/10.1017/S0022112009990954 Published online by Cambridge University Press

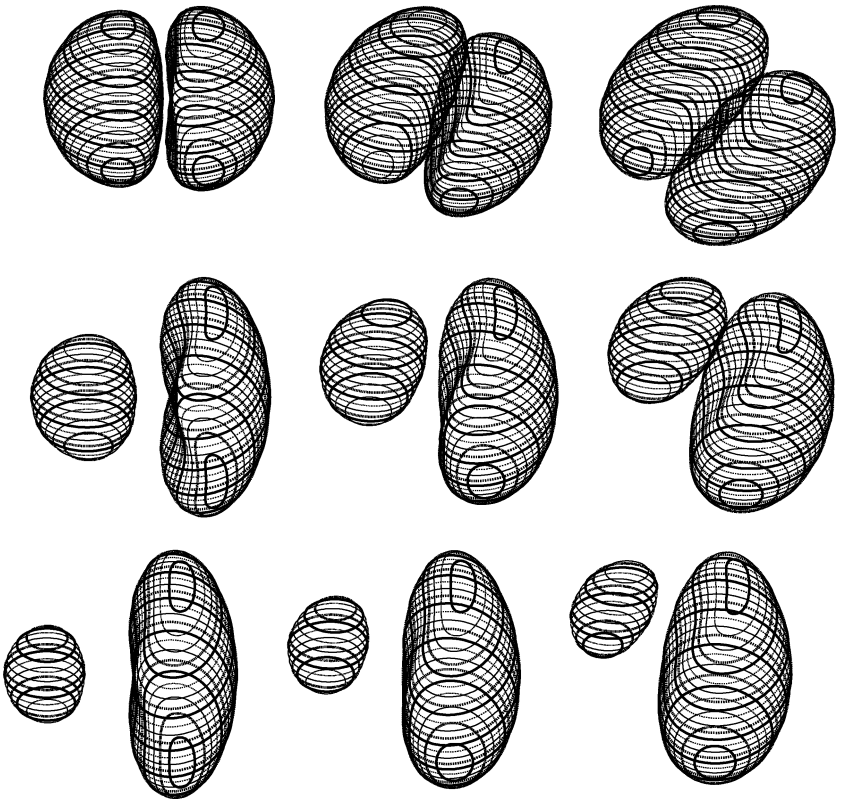


FIGURE 3. Last equilibrium states obtained numerically; for details see the caption of the previous figure.

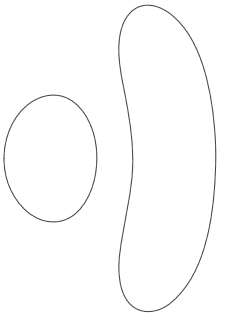


FIGURE 4. Illustration of the departure from ellipsoidal shape: cross-section in the plane $z=0$ of the last steady state obtained for $\rho_V=4$ and $\Delta z=0$.

reach. Here one can see that the largest vortex exhibits a concave innermost edge, at least for the most deformed layers. This is again in sharp contrast to co-rotating vortices, which remain convex for all separation distances.

This concave deformation is most visible in the plane $z=0$, shown in figure 4 for the last steady state obtained for $\rho_V=4$ and $\Delta z=0$. The cross-section of vortex 2 exhibits a bean shape, while the smaller vortex is closer to an ellipsoid. The bean shape of vortex 2 is not well fit by an ellipse, and this explains why numerical studies

https://doi.org/10.1017/S0022112009990954 Published online by Cambridge University Press

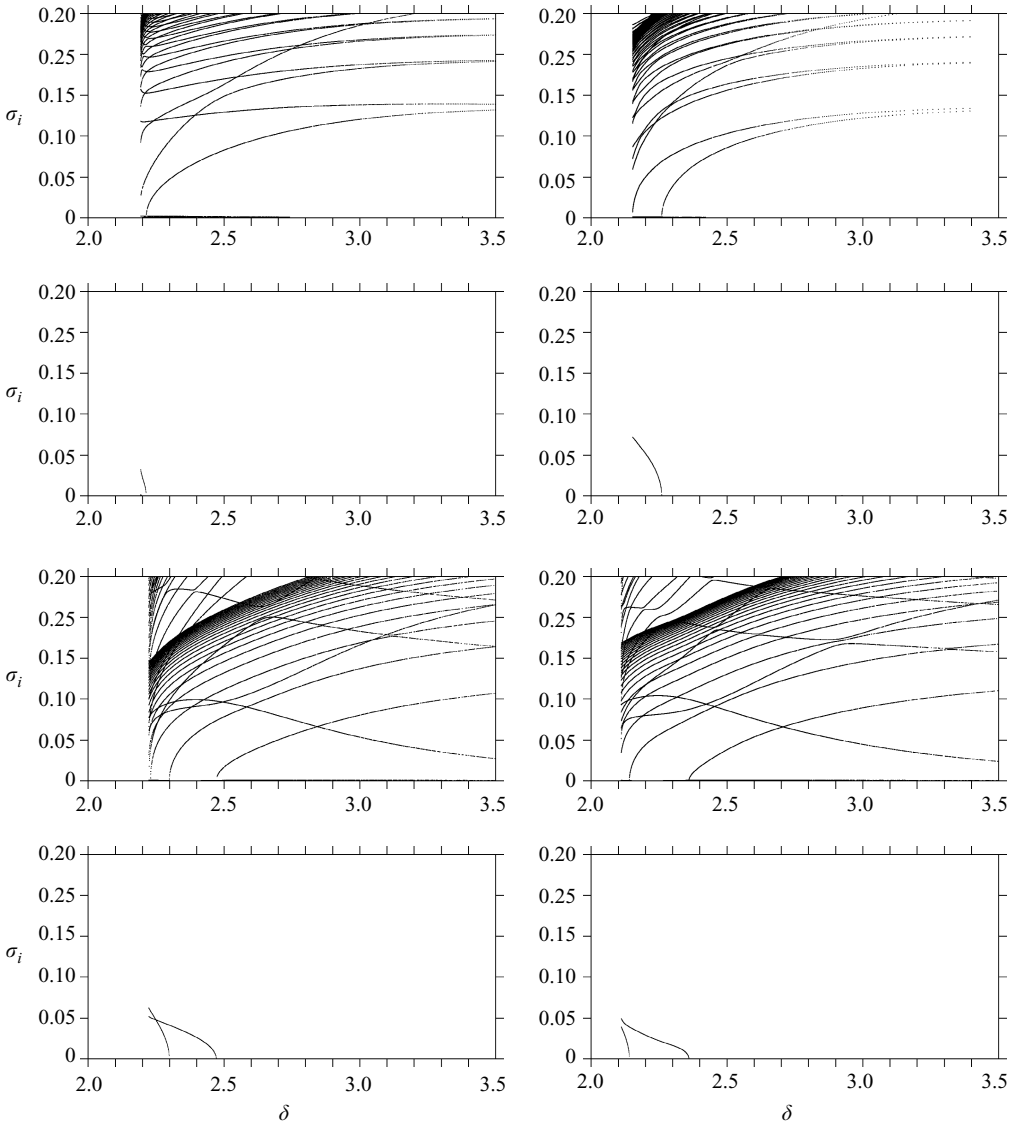


FIGURE 5. Frequencies (σ_i) and growth rates (σ_r) of the instability modes as functions of the outermost gap between the two vortices. The four top figures correspond to the volume ratios of 1.01 and the four bottom figures to the volume ratios of 10. The left column corresponds to no vertical offset and the right-column corresponds to $\Delta z = 0.5(h_1 + h_2)$.

based on ellipsoidal models alone failed to accurately reproduce the exact equilibrium states and their stability properties (cf. Miyazaki *et al.* 2003) .

We now turn to the linear stability analysis of the modes for these configurations. When vortices are well separated their mutual influence is weak and the equilibrium is neutrally stable. Below a critical separation distance, the first unstable mode appears. We can continue the family of equilibria beyond this margin of stability and observe secondary instabilities for closer vortices. Figure 5 shows the evolution of the complex eigenvalues $\sigma = \sigma_r + \mathrm{i}\sigma_i$ as a function of the outermost gap δ. The real part σ_r of the mode corresponds to the growth rate of the eigenmode, while the imaginary part

https://doi.org/10.1017/S0022112009990954 Published online by Cambridge University Press

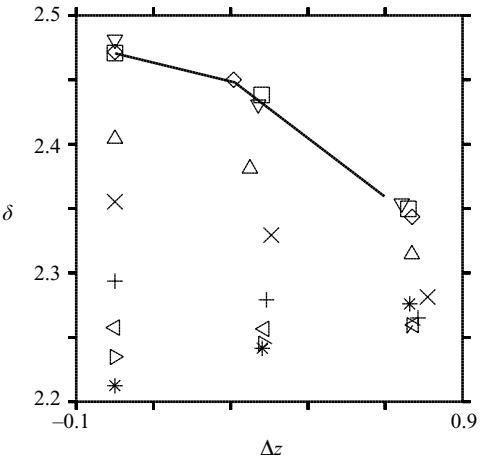


FIGURE 6. Critical gap δ against the vertical offset Δz for volume ratios 1.01 ($*$), 1.05 ($\triangleright$), 1.1 ($\triangleleft$), 1.2 ($+$), 1.5 ($\times$), 2 ($\triangle$), 4 ($\triangledown$), 6 ($\square$), 8 ($\diamond$), 10 (thick solid line).

σ_i corresponds to the frequency. We illustrate $\sigma(\delta)$ for the volume ratios $\rho_V = 1.01$ and 10 and vertical offsets $\Delta z = 0$ and $0.5(h_1 + h_2)$. These graphs are characteristic of all situations encountered. Before the margin of stability ($\delta > \delta_c$), all growth rates are zero, and therefore all modes are neutrally stable. Neutral modes come in pairs, in the sense that if $\sigma = \sigma_i$ is a solution to the eigenproblem, $\sigma = -\sigma_i$ is also a solution. One pair of modes has a frequency that decreases fastest as δ is decreased. Eventually the frequency collapses to zero at a critical gap δ_c, and the eigenvalue becomes real beyond that gap. This means that this pair of modes which was a propagating, neutral mode (with purely imaginary eigenvalues) for $\delta > \delta_c$ becomes a pair of non-propagating stable/unstable modes (modes with $\sigma = \pm\sigma_r$) for $\delta < \delta_c$. Such instability is referred to as exchange-type instability. A similar situation is observed for co-rotating vortices (see Reinaud & Dritschel 2002). Yet, in contrast to the co-rotating situation, the emergence of the instability at $\delta = \delta_c$ does not correspond to an extremum for the total energy or for the angular impulse of the family of equilibria. The physical mechanism behind the linear instability is the usual vortical Rossby wave resonance, where waves on the two vortices become phase locked (hence $\sigma_i = 0$). This is generic in vortex stability (see Reinaud & Dritschel 2002 for co-rotating vortices).

We note that sub-dominant modes, following the same scenario, are also often observed, but their growth rates typically remain smaller than that of the dominant one except for a few equilibrium states at the smallest gaps describing a family.

We next show in figure 6 the critical gap δ_c versus the vertical offset Δz for all the volume ratios ρ_V considered. Overall, the average critical gap $\bar{\delta_c} \simeq 2.35$. Recall that the length scale of the problem, $\ell = 1$, is implicitly set by the total volume of the PV, $V_{tot} = 4\pi/3$. Remarkably, in the parameter space studied, the extreme values for δ_c, which are observed for $\Delta z = 0$, only vary from $\delta_c = 2.21$ for $\rho_V = 1.01$ to $\delta_c = 2.48$ for $\rho_V = 4$. Hence the maximum relative deviation for δ_c is only 11.5 %, despite the significant difference in volume ratios between these cases.

For the volume ratio $\rho_V = 1.1$, the critical gap $\delta_c \simeq 2.26$ is almost independent of the vertical offset Δz. For $\rho_V < 1.1$, δ_c increases with Δz. In these cases, vortices have a similar strength (volume integral of their PV). To sustain a mutual equilibrium, the vortices have to tilt significantly from an upright standing position when Δz is

https://doi.org/10.1017/S0022112009990954 Published online by Cambridge University Press

increased, as illustrated in figure 2 (top row). Then their outermost-edge separation distance δ increases as Δz increases.

On the other hand δ_c decreases with Δz for $\rho_v > 1.1$. There, the asymmetry of strength between the vortices is greater. As a consequence, the tilt angle of the vortices is reduced, as vortex 1 has less influence on vortex 2 (see the middle and bottom rows of figure 2). When the vortices are offset in the vertical their mutual influence weakens for a given gap; hence the margin of stability corresponds to a smaller gap. We also note that δ_c is nearly independent of the volume ratio for $\rho_V \geqslant 4$. This shows that the outermost edge separation distance δ is a good measure of opposite-signed vortex interactions. For $\rho_V \geqslant 4$, we note $\sqrt{\Delta z^2 + {\delta_c}^2} \sim$ constant. This distance corresponds roughly to the separation distance r between the two vortices. The collapse of the data on to this curve suggests that instability results from excessive shear ($\propto r^{-3}$) induced by the 'smaller' vortex on the larger one. As discussed in the following section, in all such cases the larger vortex strongly destabilizes, while the smaller vortex remains intact.

4. Nonlinear evolution

4.1. *Numerical approach*

We next focus on the outcome of the nonlinear evolution of unstable equilibria, for a small subset of the results presented in the previous section. We use the purely Lagrangian CS algorithm (Dritschel 1988), rather than the lower-cost CASL algorithm (Dritschel & Ambaum 1997), to be consistent with the numerical approach used to determine the equilibrium states in an infinite domain. This also avoids any effects of periodicity associated with the CASL algorithm. Details on CS for three-dimensional QG flows may be found in Dritschel (2002) and Reinaud & Dritschel (2002).

We start the simulations with unstable equilibrium states. To determine the equilibria, we used a fine discretization of each contour (namely 198 nodes) to be able to accurately capture the shape of the equilibrium states. From experience low resolution does not allow one to find as many states and is less accurate. Such a high spatial discretization is however impractical for the investigation of the nonlinear evolution, due to computational cost. In CS, we use a renoding procedure which minimizes and redistributes the number of nodes discretizing each contour (see Dritschel 1988; Dritschel & Ambaum 1997). While this still represents the contours accurately, the node redistribution induces a small disturbance to the contours at all azimuthal wavenumbers available and therefore seeds any instabilities.

We analyse the development of the interaction by identifying in the flow all individual coherent vortical structures. These coherent structures are defined as contiguous (compact) volumes of the PV. Using contour integration we can calculate various properties of these structures. In particular, we measure their volume to quantify how much material the initial vortices may lose following a strong interaction.

4.2. *Results*

We first illustrate the interaction of two horizontally aligned opposite-signed vortices with a volume ratio of $\rho_V = 1.01$. The vortices initially reside at the margin of stability, $\delta_c = 2.2124$. Each vortex is spanned by 25 layers. The vortices remain close to equilibrium for a long time, while weak disturbances amplify. Then, vortex 2, the bigger vortex, tilts and is sheared around vortex 1. This is illustrated in figure 7 (top row). We note that the deformed vortices are no longer symmetric with respect to the plane $z = 0$. Small filaments and debris detach by $t = 139$. At $t = 142.25$, a large

https://doi.org/10.1017/S0022112009990954 Published online by Cambridge University Press

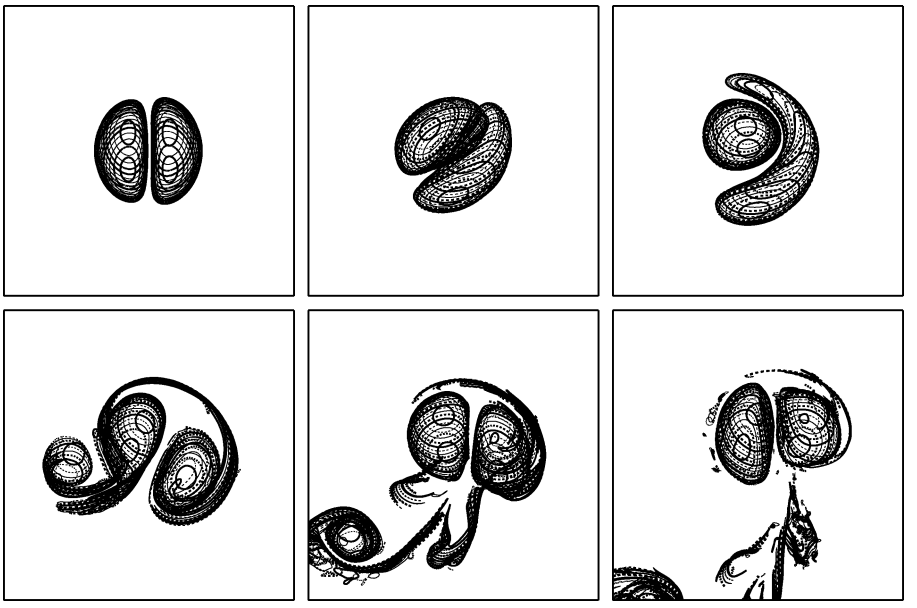


FIGURE 7. Time evolution of opposite-signed vortices with $\Delta z = 0$ and $\rho_V = 1.01$, at times $t = 0$, 130, 135, 140, 145, 150 (left to right and top to bottom). The initial conditions consist of vortices at the margin of stability. Vortices are viewed orthographically at an angle of 30° from the vertical. Views are centred at the volume centroid.

satellite vortex is torn from vortex 2. The satellite vortex represents 5.5 % of the initial volume of vortex 2. Rapidly a large number of filaments are also formed. By $t = 150$, vortex 2 has lost 29 % of its volume. By comparison, vortex 1 loses 6 % of its volume, and therefore is the largest vortex at the end of the simulation. The largest two vortices only weakly interact thereafter.

Note that the total energy of a vortex

$$E = -\frac{1}{2}\iiint q\psi \mathrm{d}V, \tag{4.1}$$

can be related to the vortex volume V, for compact vortices which, at leading order in deformation, may be approximated by a spherical shape. The energy of a spherical vortex of uniform PV $q = Q$ and volume V is $E = (4\pi Q^2/15)r^5 \propto Q^2V^{5/3}$, using $r = (3V/4\pi)^{1/3}$ for the vortex radius. In spectral space, this energy resides around a wavenumber $k \propto 1/r$. Therefore the analysis of vortex volume changes gives a simple qualitative method for estimating energy transfers in physical space. (The smaller the vortex, the less energy it contains.) The vortex interaction energy, neglected here, is comparatively small based on previous analyses of QG vortex interactions (Reinaud & Dritschel 2002).

We next illustrate in figure 8 the strong interaction between an unstable pair of vortices for the same volume ratio but offset vertically by $\Delta z \simeq 0.5(h_1 + h_2)$. Recall that vortex 1 (the smaller vortex) is on the top. We start with vortices beyond the margin of stability such that the growth rate of the most unstable mode is significant. We take $\delta = 2.2512$, while the margin of stability is $\delta_c = 2.2760$. At $t = 600$, we see that vortex 2 has been significantly distorted. It has been elongated, and its upper part has been sheared by vortex 1. This is the part of vortex 2 most likely to strongly interact with vortex 1, as it resides on layers that both vortices have in common.

https://doi.org/10.1017/S0022112009990954 Published online by Cambridge University Press

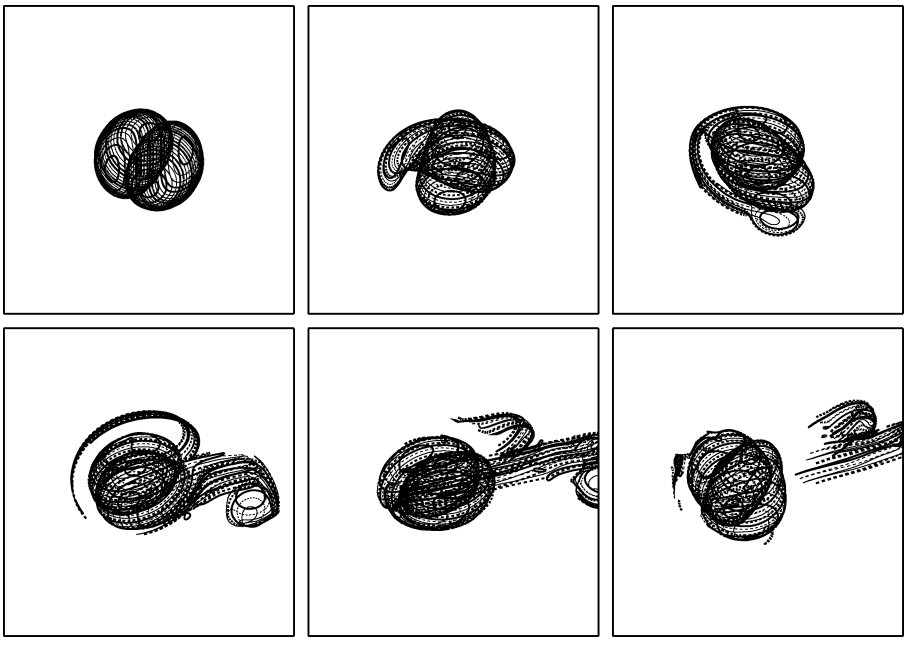


FIGURE 8. Time evolution of opposite-signed vortices with $\Delta z \simeq 0.5(h_1 + h_2)$ and $\rho_V = 1.01$, at times $t = 0$, 600, 605, 609.25, 612.5, 616.25. See the caption of figure 7 for details.

The subsequent evolution of the interaction is rapid. At $t = 609.25$ a large structure is expelled, mostly composed of the PV from vortex 2. It corresponds to 12.5 % of the volume of vortex 2 at $t = 0$. This material leaves the pair, and the pair remains metastable afterwards only throwing out limited amounts of debris from time to time. The main difference in the flow evolution from the previous case stems from the vertical offset which brings an additional asymmetry: vortices are tilted from the vertical axis from the start. Therefore, the nonlinear evolution of the vortices is more asymmetric, and the top of vortex 2 deforms the most.

The next example consists of a pair of vortices with a volume ratio $\rho_V = 4$ and no vertical offset, $\Delta z = 0$. This increases the asymmetry in the initial conditions between the two vortices from the case with $\rho_V = 1.01$. As in the previous case, we start beyond the margin of stability to intensify the interaction, with a gap $\delta = 2.2843$ (note $\delta_c = 2.4813$). In this case, the growth rate of the most unstable mode is $\sigma_r = 0.0588$. The evolution of the flow is presented in figure 9. Again, vortex 2 exhibits the largest deformation as it is stretched by vortex 1. By $t = 25$, the last time frame shown, there are 41 identifiable structures. Vortex 1 still retains 98.2 % of its volume and has not been further affected by the interaction. On the other hand, vortex 2 has been more strongly affected, retaining only 88.9 % of its initial volume. The largest satellite vortex has increased in volume to 5.54 % of the volume of vortex 1 at $t = 0$. Later on, the situation remains similar with an increasing amount of small debris.

We now consider the same volume ratio $\rho_V = 4$ but a vertical offset $\Delta z \simeq 0.5(h_1 + h_2)$. This case is shown in figure 10. Recall that vortex 1 is on the top. The initial conditions consist of an unstable equilibria for $\delta = 2.2323$ (here $\delta_c = 2.3539$ and $\sigma_r = 0.0254$). As in all previous cases, vortex 2 exhibits the largest deformation. At $t = 45$, vortex 2 contains 96.6 % of its initial volume, while vortex 1 still contains 99.6 % of its initial

https://doi.org/10.1017/S0022112009990954 Published online by Cambridge University Press

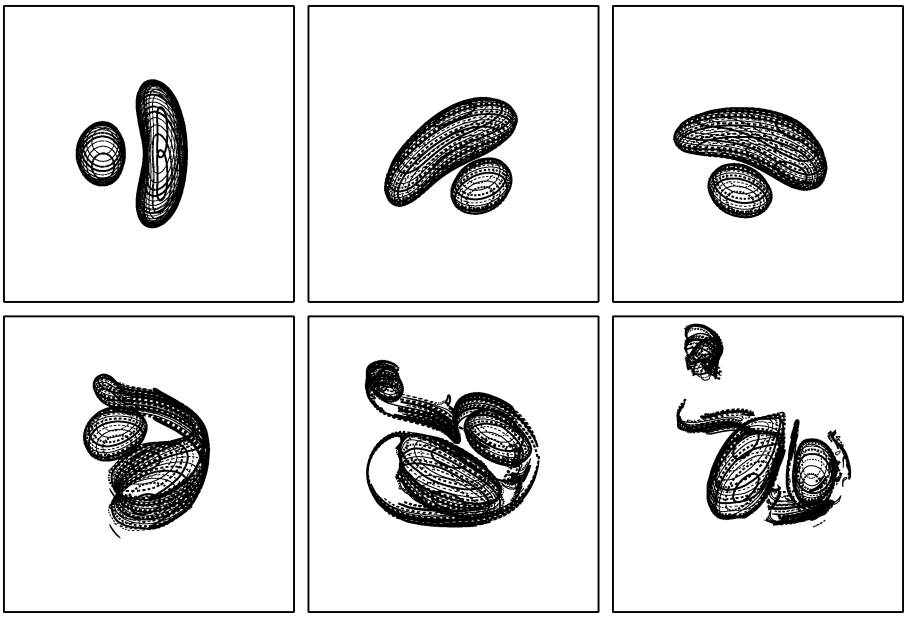


FIGURE 9. Time evolution of opposite-signed vortices with $\Delta z = 0$ and $\rho_V = 4$, at times $t = 0,\ 10,\ 12.5,\ 17.5,\ 22.5,\ 25$. See the caption of figure 7 for details.

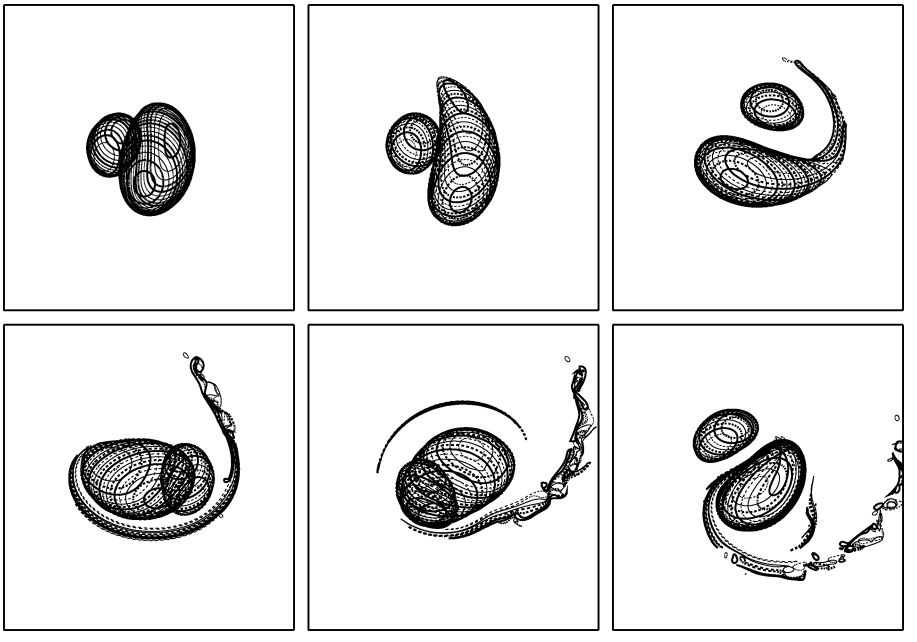


FIGURE 10. Time evolution of opposite-signed vortices with $\Delta z \simeq 0.5(h_1 + h_2)$ and $\rho_V = 4$, at times $t = 0,\ 25,\ 30,\ 35,\ 40,\ 45$. See the caption of figure 7 for details.

volume. The largest tertiary vortex represents in volume 2.6 % of the initial volume of vortex 1. Although this interaction is weaker than those illustrated previously, it consistently shows the stronger destabilization of vortex 2, the 'larger' vortex, which is partially sheared.

https://doi.org/10.1017/S0022112009990954 Published online by Cambridge University Press

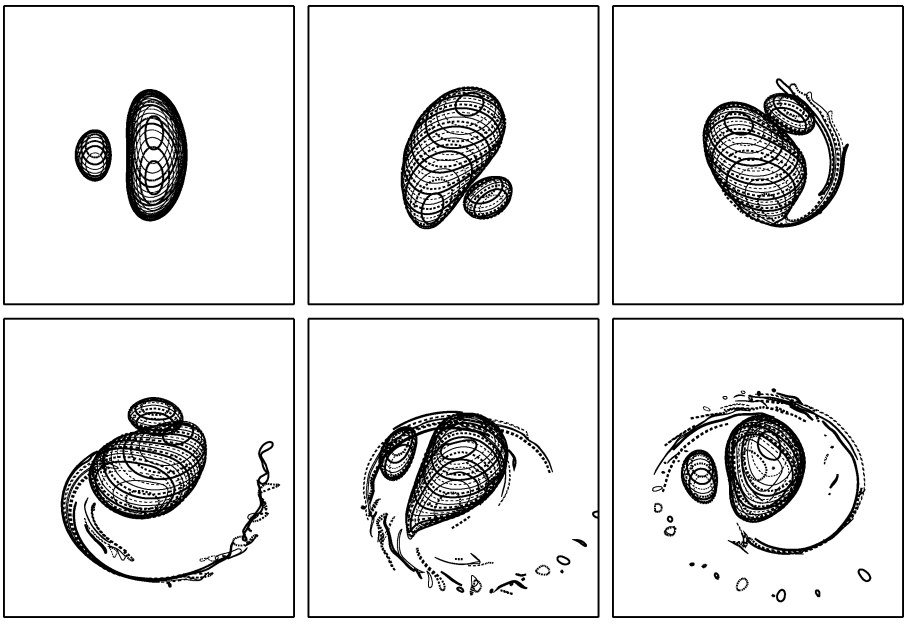


FIGURE 11. Time evolution of opposite-signed vortices with $\Delta z = 0$ and $\rho_V = 10$, at times $t = 0$, 90, 100, 110, 120, 130. See the caption of figure 7 for details.

In our final set of examples, we illustrate interactions typifying large volume ratios, $r_V = 10$. In the first example, we consider vortices horizontally aligned ($\Delta z = 0$). The evolution of the interaction is shown in figure 11. The horizontal gap between the two vortices is $\delta = 2.2978$ (here $\delta_c = 2.4706$ and $\sigma_r = 0.0413$). At $t = 130$, vortex 2 has lost about 2.8 % of its volume, while vortex 1 has lost only 0.2 % of its initial volume.

The last example illustrates the strong interaction between two vortices with $\rho_V = 10$ and a vertical offset $\Delta z = 0.5(h_1 + h_2)$. The gap between the two vortices is initially $\delta = 2.1107$ (here $\delta_c = 2.3595$ and $\sigma_r = 0.0493$). The vortex evolution is shown in figure 12. We notice that initially, due to the vertical offset, the top of vortex 2 is significantly more deformed than the bottom. Hence, it is likely that the top of the vortex will destabilize first. As seen in figure 12, a filament of the PV is shredded from the top of the vortex. As in the previous case ($\rho_V = 10$, $\Delta z = 0$), the tail of the filament destabilizes and breaks into small-scale structures. Remarkably, in this case the filament shredded from vortex 2 only surrounds vortex 1 and does not strongly interact with it; in other words vortex 1 is never in direct contact with the other vortices and retains its volume. By $t = 60$, vortex 2 has lost 4 % of its volume. The PV lost is mostly within 117 identifiable individual small-scale structures in the flow, the largest containing only about 1.5 % of the volume of vortex 1. Again, the main difference here from the previous case with the same volume ratio is the additional asymmetry brought by the vertical offset between the two vortices. The top of vortex 2 becomes rapidly more deformed than its bottom, due to its proximity to vortex 1.

We have simulated several tens of other cases, for various volume ratios and vertical offsets, and in all cases we have found destructive interactions, principally characterized by a 'reduction' in the size of the largest vortex. Hence, in general, opposite-signed vortices can – and do – interact destructively. In contrast to strong interactions between like-signed vortices, those between opposite-signed vortices 'always lead to smaller vortices' and filamentary debris.

https://doi.org/10.1017/S0022112009990954 Published online by Cambridge University Press

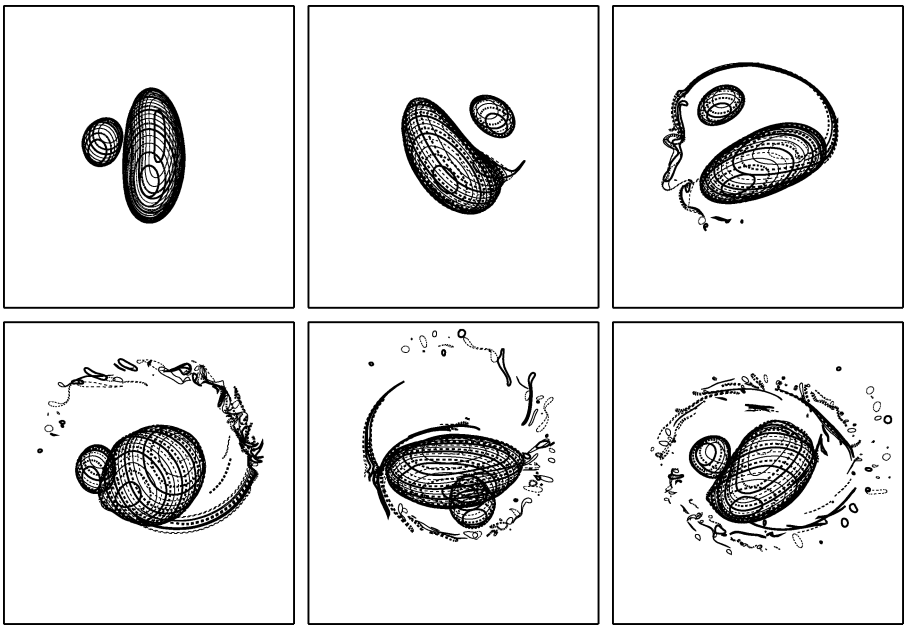


FIGURE 12. Time evolution of opposite-signed vortices with $\Delta z \simeq 0.5(h_1 + h_2)$ and $\rho_V = 10$, at times $t = 0,\ 15,\ 25,\ 35,\ 45,\ 60$. See the caption of figure 7 for details.

5. Conclusions

In this study, we have illustrated the destructive interaction between two counter-rotating (opposite-signed) QG vortices for various volume ratios and vertical offsets between the vortices. For the sake of simplicity we have restricted attention to vortices having a mean height-to-width aspect ratio of one. This restriction is partially justified by simulations of QG turbulence (Reinaud *et al.* 2003), where vortices have an order-one height-to-width aspect ratio in vertically stretched coordinates $(x, y, Nz/f)$.

We have found it essential to compute equilibrium states using the full QG equations. Lower-cost asymptotic models (such as ellipsoidal models) fail to capture any instability.

In the full equations, all families of equilibria become unstable for a sufficiently small gap between the outermost edges of the vortices. The critical gap δ_c, corresponding to the margin of stability, varies only weakly as a function of the volume ratio and the vertical offset. Over the parameter space considered, the maximum variation is observed for horizontally aligned vortices and represent 11.5 % of the overall mean critical gap $\bar{\delta_c} = 2.35$ (taking the sum of the vortex volumes to be $4\pi/3$). This variation decreases as the vertical offset increases. We also note that δ_c tends to become independent of the volume ratio for $\rho_V \geqslant 4$. As far as the shape of the equilibrium states is concerned, we have consistently found that the largest vortex is the most deformed.

During the nonlinear evolution of unstable equilibria, we see that initially the largest vortex starts to tilt and is sheared by the smaller vortex. This deformation causes the largest vortex to break asymmetrically. As illustrated in the examples detailed in § 4.2, and from additional experiments, the interaction is more destructive for vortices having similar volume. In these cases, the mutual deformation is more intense and

https://doi.org/10.1017/S0022112009990954 Published online by Cambridge University Press

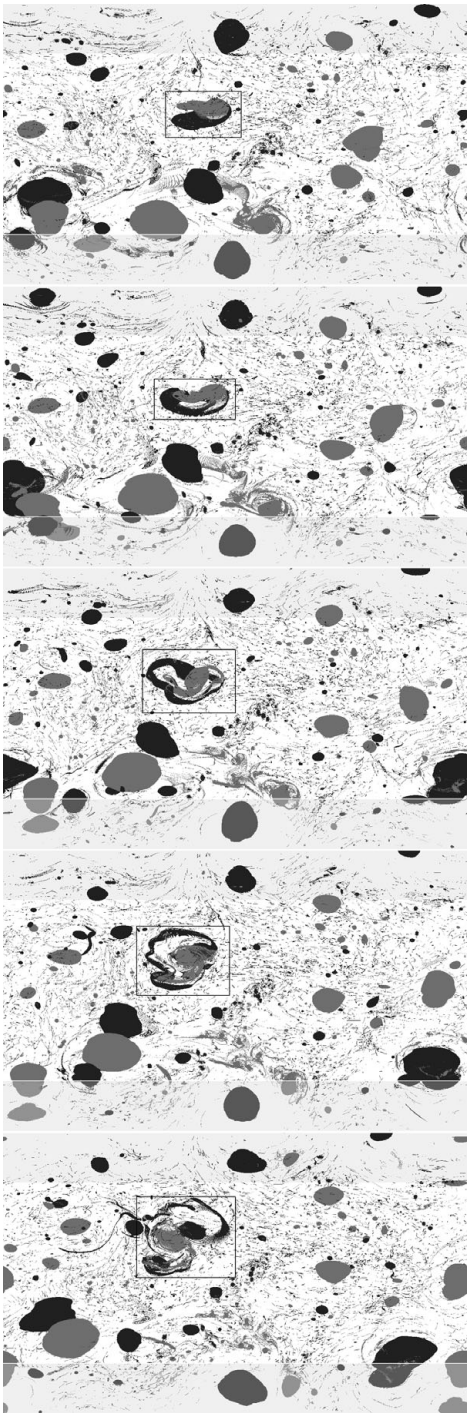


FIGURE 13. Turbulence simulation: an example of a destructive interaction between opposite-signed vortices. Only an eighth of the domain in shown, from layer 129 to layer 256 in the 1024^3 domain. From top to bottom, times displayed are $t = 465$, 467.5, 470, 472.5 and 476.5.

https://doi.org/10.1017/S0022112009990954 Published online by Cambridge University Press

durable. However in every situation, the largest vortex loses at least a small fraction of its initial volume.

Hence opposite-signed interactions produce smaller scales, not larger ones. In turbulence, such interactions therefore likely contribute principally to a direct energy cascade. This result, together with results for co-rotating vortices (Ozugurlu *et al.* 2008), shows the limitation of the commonly accepted idea that the spectral inverse energy cascade observed in QG turbulence can be directly associated with the exchange of material between vortices during their strong interactions. Many such interactions generate smaller vortices.

We have examined this conjecture by conducting a high-resolution CASL simulation of QG turbulence in a triply periodic box, using initial conditions similar to those used in Reinaud *et al.* (2003). Here the fine grid is 1024^3, with a coarse (or inversion) grid of 256^3. Initially, 800 spherical vortices of uniform PV ($q = \pm 4\pi$) and of equal volume, occupying altogether 7.5 % of the domain, are placed randomly (without overlapping). In time, the flow rapidly grows in complexity. Many strong interactions occur, including the merger of like-signed vortices but also the destructive interaction of vortex pairs. One example is shown in figure 13. Here, a vortex pair forms near the centre and breaks down into smaller vortices and debris in just two or three typical vortex rotation periods. Such examples are widespread in this simulation and indicate at the very least that vortex interactions are considerably more complex than previously imagined.

Finally, for simplicity this and many previous studies of vortex interactions have employed the QG approximation, valid for small Rossby and Froude numbers $Ro \sim Fr \ll 1$. However, remarkably little is known for $O(1)$ values of Ro and Fr. It is important to lift this restriction, in order to consider ageostrophic effects which break the symmetry between cyclonic and anticyclonic vortices. In the atmosphere and oceans, ageostrophic effects are thought to play an important role at small-to-intermediate scales, where rotation and stratification have less control on fluid motions than at large scales. Therefore, to better understand fluid motions at smaller scales, a necessary step is to go beyond the QG and use more accurate descriptions of atmospheric and oceanic dynamics.

The authors thank Professor Xavier Carton for helpful comments on the manuscript.

REFERENCES

Bambrey, R. R., Reinaud, J. N. & Dritschel, D. G. 2007 Strong interactions between two co-rotating quasi-geostrophic vortices. *J. Fluid Mech.* **592**, 117–133.

Dritschel, D. G. 1988 Contour surgery: a topological reconnection scheme for extended integrations using contour dynamics. *J. Comput. Phys.* **77**, 240–266.

Dritschel, D. G. 1995 A general theory for two-dimensional vortex interactions. *J. Fluid Mech.* **293**, 269–303.

Dritschel, D. G. 2002 Vortex merger in rotating stratified flows. *J. Fluid Mech.* **455**, 83–101.

Dritschel, D. G. & Ambaum, M. H. P. 1997 A contour-advective semi-Lagrangian algorithm for the simulation of fine-scale conservative fields. *Quart. J. R. Met. Soc.* **123**, 1097–1130.

Ebbesmeyer, C. C., Taft, B. A., McWilliams, J. C., Shen, C. Y., Riser, S. C., Rossby, H. T., Biscaye, P. E. & Östlund, H. G. 1986 Detection, structure and origin of extreme anomalies in a western atlantic oceanographic section. *J. Phys. Oceanogr.* **16**, 591–612.

Garrett, C. 2000 The dynamic ocean, In *Perspectives in Fluid Dynamics* (ed. G. K. Batchelor, H. K. Moffatt & M. G. Worster), chap. 10, pp. 507–553. Cambridge University Press.

https://doi.org/10.1017/S0022112009990954 Published online by Cambridge University Press

von Hardenberg, J., McWilliams, J. C., Provenzale, A., Shchpetkin, A. & Weiss, J. B. 2000 Vortex merging in quasi-geostrohic flows. *J. Fluid Mech.* **412**, 331–353.

Holton, J. R., Haynes, P. H., McIntyre, M. E., Douglass, A. R., Rood, R. B. & Pfister, L. 1995 Stratosphere–troposphere exchange. *Rev. Geophys.* **33** (4), 403–439.

Hua, B. L. & Haidvogel, D. B. 1986 Numerical simulations of the vertical structure of quasi-geostrophic turnulence. *J. Atmos. Sci.* **43** (23), 2923–2936.

McWilliams, J., Weiss, J. & Yavneh, I. 1999 The vortices of homogeneous geostrophic turbulence. *J. Fluid Mech.* **401**, 1–26.

Miyazaki, T., Yamamoto, M. & Fujishima, S. 2003 Counter-rotating quasigeostrophic ellipsoidal vortex pair. *J. Phys. Soc Jpn* **72** (8), 1942–1953.

Ozugurlu, E., Reinaud, J. N. & Dritschel, D. G. 2008 Interaction between two quasi-geostrophic vortices of unequal potential-vorticity. *J. Fluid Mech.* **597**, 395–414.

Reinaud, J. N. & Dritschel, D. G. 2002 The merger of vertically offset quasi-geostrophic vortices. *J. Fluid Mech.* **469**, 287–315.

Reinaud, J. N. & Dritschel, D. G. 2005 The critical merger distance between two co-rotating quasi-geostrophic vortices. *J. Fluid Mech.* **522**, 357–381.

Reinaud, J. N., Dritschel, D. G. & Koudella, C. R. 2003 The shape of the vortices in quasi-geostrophic turbulence. *J. Fluid Mech.* **474**, 175–192.

Vallis, C. 2006 *Atmospheric and Oceanic Fluid Dynamics: Fundamentals and Large-Scale Circulation*. Cambridge University Press.

https://doi.org/10.1017/S0022112009990954 Published online by Cambridge University Press